

Thermoelastic bending analysis of functionally graded sandwich plates

Ashraf M. Zenkour · N. A. Alghamdi

Received: 8 July 2007 / Accepted: 15 January 2008 / Published online: 20 February 2008
© Springer Science+Business Media, LLC 2008

Abstract The thermoelastic bending analysis of functionally graded ceramic–metal sandwich plates is studied. The governing equations of equilibrium are solved for a functionally graded sandwich plates under the effect of thermal loads. The sandwich plate faces are assumed to have isotropic, two-constituent material distribution through the thickness, and the modulus of elasticity, Poisson’s ratio of the faces, and thermal expansion coefficients are assumed to vary according to a power law distribution in terms of the volume fractions of the constituents. The core layer is still homogeneous and made of an isotropic ceramic material. Several kinds of sandwich plates are used taking into account the symmetry of the plate and the thickness of each layer. Field equations for functionally graded sandwich plates whose deformations are governed by either the shear deformation theories or the classical theory are derived. Displacement functions that identically satisfy boundary conditions are used to reduce the governing equations to a set of coupled ordinary differential equations with variable coefficients. The influences played by the transverse normal strain, shear deformation, thermal load, plate aspect ratio, side-

to-thickness ratio, and volume fraction distribution are studied. Numerical results for deflections and stresses of functionally graded metal–ceramic plates are investigated.

Introduction

Sandwich construction has been developed and utilized for almost 50 years because of its outstanding bending rigidity, low specific weight, superior isolating qualities, excellent vibration characteristics, and good fatigue properties. The first two characteristics are the major reasons that it is used more often in aerospace vehicles, which need high strength-to-weight ratio. Recently, sandwich construction became even more attractive due to the introduction of advanced composite materials for the faces. In the design of sandwich skins for aircraft wings, one of the important issues is the bending of the plates. High-speed aircraft structural plates are subjected not only to aerodynamic loading, but also to aerodynamic heating. The temperature rise may bend the plate and exhaust the load carrying capacity. The current trend in the design and development of highly heated sandwich plates in the aerospace and automobile industries is to use advanced sandwich, such as Titanium–Zirconia sandwich plates. These materials provide excellent thermo mechanical properties at elevated temperatures. In view of the fact that the demand for these materials is growing, there is a necessity to understand the thermo-structural behavior of structural elements made out of these materials, and to evolve appropriate design and analysis methodologies.

Thermal stress analysis of isotropic structures fascinated several post-war researchers. Significant contributions were made by Timoshenko and Woinowsky-Krieger [1], Nowacki [2], and Boley and Weiner [3]. Most of the

A. M. Zenkour (✉)
Department of Mathematics, Faculty of Science,
King AbdulAziz University, P.O. Box 80203, Jeddah 21589,
Saudi Arabia
e-mail: zenkour@hotmail.com; zenkour@gmail.com

Present Address:
A. M. Zenkour
Department of Mathematics, Faculty of Education,
Kafr El-Sheikh University, Kafr El-Sheikh 33516, Egypt

N. A. Alghamdi
Department of Mathematics, College of Girl’s Education,
Holy Makkah 3653, Saudi Arabia

previous research in the field of composite structures has been concerned with isothermal problem. However, serious efforts in the thermal stress analysis of composites were made only in the eighties. An analytical method was suggested by Wu and Tauchert [4, 5] and Tauchert [6] to investigate thermal deformations in both symmetric and anti-symmetric laminates.

A simply supported rectangular homogeneous isotropic plate subjected to tent-like temperature distribution was analyzed using the Rayleigh–Ritz procedure. The critical temperatures for different types of composite have been compared with that of aluminum plate using energy formulation. Static problems associated with the linear thermo-elastic analysis of laminated plates have been studied extensively [4, 5, 7, 8]. Pell [7], who derived the equations governing the transverse deflection of a thin plate, first studied the problem of thermal bending of anisotropic plates. Generalization of this work to heterogeneous plates subjected to arbitrary three-dimensional temperature distribution is due to Stavsky [8].

Recent studies in the thermoelastic analysis of plates that are laminates of fiber-reinforced materials indicate that the shear deformation effect on the behavior of the plate is more pronounced than in isotropic plates (see, for example, Wu and Tauchert [4, 5]). Various first- and higher-order theories, originally developed for the analysis of isothermal problems of laminated plates, have been extended to include thermoelastic effects [9–17]. In fact, a shear correction factor is introduced in all of the previous first-order theories.

In this article, a unified shear deformable plate theory is developed for thermoelastic bending of FGM sandwich plates (see Zenkour [18]). This theory is simplified by enforcing traction-free boundary conditions at the plate faces. The effects of shear and normal deformations are both included. Exact solutions for homogeneous and FGM sandwich plates are presented. The effects of temperature field on the dimensionless axial and transverse shear stresses of the FGM sandwich plate are studied. Numerical results for deflection and stresses are investigated.

Problem formulation

Let us consider the case of a flat sandwich plate composed of three microscopically heterogeneous layers as shown in Fig. 1. Several assumptions to simplify the complexity of the problem are introduced. These are:

- (1) The face layers of the sandwich plate are made of a functionally graded material with material properties varying smoothly in the z (thickness) direction only.
- (2) The core layer is made of an isotropic homogeneous material.

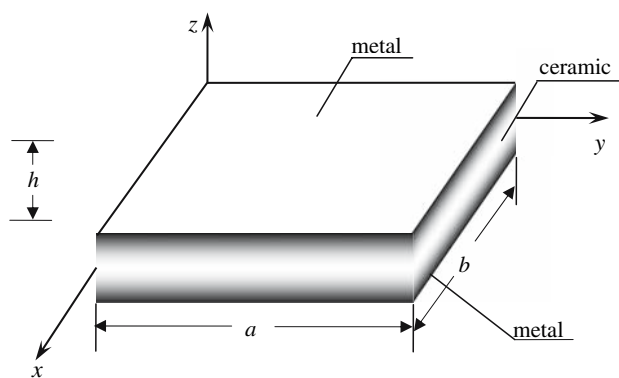


Fig. 1 Geometry of the FGM sandwich rectangular plate

- (3) The sandwich plate is symmetrical with respect to the mid plane $z = 0$.
- (4) The bottom layer of the plate is made of mixed metal–ceramic material, which is started with metal and graded to ceramic.
- (5) The core layer is a fully ceramic layer.
- (6) The top layer of the plate is made of mixed ceramic–metal material, which is started with ceramic and graded to metal.
- (7) The effective material properties for faces layers, like Young’s modulus, Poisson’s ratio, and thermal expansion coefficients, can be expressed as

$$P(z) = P_m + (P_c - P_m)V^{(n)}, \tag{1}$$

where P_m and P_c denote the property of the bottom and top faces of layer 1, respectively, and vice versa for layer 3 depending on the volume fraction $V^{(n)}(n = 1, 2, 3)$. Note that P_m and P_c are, respectively, the corresponding properties of the metal and ceramic of the FGM sandwich plate.

Rectangular Cartesian coordinates (x, y, z) are used to describe infinitesimal deformations of a three-layer sandwich elastic plate occupying the region $[0, a] \times [0, b] \times [-h/2, +h/2]$ in the unstressed reference configuration. The mid-plane of the composite sandwich plate is defined by $z = 0$ and its external bounding planes being defined by $z = \pm h/2$. The vertical positions of the bottom surface, the two interfaces between the core and faces layers, and the top surface are denoted, respectively, by $h_0 = -h/2, h_1, h_2, h_3 = h/2$.

The volume fraction $V^{(n)}$ through the thickness of the sandwich plate faces follows a simple power-law while it equals unity in the core layer. It reads

$$V^{(1)} = \left(\frac{z - h_0}{h_1 - h_0} \right)^k, \quad z \in [h_0, h_1], \tag{2a}$$

$$V^{(2)} = 1, \quad z \in [h_1, h_2], \tag{2b}$$

$$V^{(3)} = \left(\frac{z - h_3}{h_2 - h_3} \right)^k, \quad z \in [h_2, h_3], \quad (2c)$$

where k is a parameter that dictates the material variation profile through the faces thickness (the volume fraction exponent), which takes values greater than or equal to zero. The core layer is independent of the value of k which is a fully ceramic layer. However, the value of k equal to zero represents a fully ceramic plate. The above power-law assumption given in Eqs. 2a and 2c reflects a simple rule of mixtures used to obtain the effective properties of the ceramic–metal plate faces (see Fig. 1). Note that the volume fraction of the metal is high near the bottom and top surfaces of the plate, and that of ceramic is high near the interfaces. In addition, Eq. 2 indicates that the top ($z = h_3$) and bottom ($z = h_0$) surfaces of the plate are purely metal whereas the bottom ($z = h_1$) and top ($z = h_2$) surfaces of the core are purely ceramic.

The displacements of a material point located at (x, y, z) in the plate may be written as (Zenkour [18])

$$\begin{aligned} u_x(x, y, z) &= u - z \frac{\partial w}{\partial x} + \Psi(z)\varphi_x, \\ u_y(x, y, z) &= v - z \frac{\partial w}{\partial y} + \Psi(z)\varphi_y, \\ u_z(x, y, z) &= w + \Psi'(z)\varphi_z, \end{aligned} \quad (3)$$

where $u, v, w, \varphi_x, \varphi_y,$ and φ_z are independent of z and denote the displacements and rotations of the $yz, xz,$ and xy planes due to bending, respectively.

The displacement field of the classical thin plate theory (CLPT) is obtained easily by setting $\Psi(z) = 0$ and $\varphi_z = 0$. The displacement field of the first-order shear deformation plate theory (FSDPT) is obtained by setting $\Psi(z) = z$ and $\varphi_z = 0$. Also, the displacement field of the third-order shear deformation plate theory (TSDPT) of Reddy [19] is obtained by setting

$$\Psi(z) = z \left[1 - \frac{4}{3} \left(\frac{z}{h} \right)^2 \right] \quad \text{and} \quad \varphi_z = 0. \quad (4)$$

In addition, the displacement field of the simple sinusoidal shear deformation plate theory of Zenkour [20–25] is obtained by setting

$$\Psi(z) = \frac{h}{\pi} \sin\left(\frac{\pi z}{h}\right) \quad \text{and} \quad \varphi_z = 0. \quad (5)$$

The displacement field of the present refined sinusoidal shear deformation plate theory (SSDPT) with $\varphi_z \neq 0$ is simplified by enforcing traction-free boundary conditions at the plate faces. It contains one dependent unknowns more than that in the first- and third-order shear deformation theories, but accounts according to cosine-law distribution of the transverse shear strains through the thickness of the plate. No transverse shear correction

factors are needed for both SSDPT and TSDPT because a correct representation of the transverse shearing strain is given. In addition, the effect of normal deformation is included in the present theory.

The strain components are related to the displacements given in Eq. 3 can be expressed as

$$\begin{Bmatrix} \varepsilon_x \\ \varepsilon_y \\ \gamma_{xy} \end{Bmatrix} = \begin{Bmatrix} \varepsilon_x^0 \\ \varepsilon_y^0 \\ \gamma_{xy}^0 \end{Bmatrix} + z \begin{Bmatrix} \kappa_x \\ \kappa_y \\ \kappa_{xy} \end{Bmatrix} + \Psi(z) \begin{Bmatrix} \eta_x \\ \eta_y \\ \eta_{xy} \end{Bmatrix}, \quad (6a)$$

$$\varepsilon_z = \Psi''(z)\varepsilon_z^0, \quad (6b)$$

$$\begin{Bmatrix} \gamma_{yz} \\ \gamma_{xz} \end{Bmatrix} = \Psi'(z) \begin{Bmatrix} \gamma_{yz}^0 \\ \gamma_{xz}^0 \end{Bmatrix}, \quad (6c)$$

where

$$\begin{aligned} \varepsilon_x^0 &= \frac{\partial u}{\partial x}, \quad \varepsilon_y^0 = \frac{\partial v}{\partial y}, \quad \varepsilon_z^0 = \varphi_z, \\ \gamma_{yz}^0 &= \left(\varphi_y + \frac{\partial \varphi_z}{\partial y} \right), \quad \gamma_{xz}^0 = \left(\varphi_x + \frac{\partial \varphi_z}{\partial x} \right), \\ \gamma_{xy}^0 &= \frac{\partial v}{\partial x} + \frac{\partial u}{\partial y}, \quad \kappa_x = -\frac{\partial^2 w}{\partial x^2}, \quad \kappa_y = -\frac{\partial^2 w}{\partial y^2}, \quad \kappa_{xy} = -2\frac{\partial^2 w}{\partial x \partial y}, \\ \eta_x &= \frac{\partial \varphi_x}{\partial x}, \quad \eta_y = \frac{\partial \varphi_y}{\partial y}, \quad \eta_{xy} = \frac{\partial \varphi_y}{\partial x} + \frac{\partial \varphi_x}{\partial y}. \end{aligned} \quad (7)$$

The stress–strain relationships accounting for transverse shear deformation and thermal effects for the n th layer can be expressed as

$$\begin{Bmatrix} \sigma_{xx} \\ \sigma_{yy} \\ \sigma_{zz} \\ \tau_{xy} \end{Bmatrix}^{(n)} = \begin{bmatrix} \frac{E}{1-\nu^2} & \frac{\nu E}{1-\nu^2} & \frac{\nu E}{1-\nu^2} & 0 \\ \frac{\nu E}{1-\nu^2} & \frac{E}{1-\nu^2} & \frac{\nu E}{1-\nu^2} & 0 \\ \frac{\nu E}{1-\nu^2} & \frac{\nu E}{1-\nu^2} & \frac{E}{1-\nu^2} & 0 \\ \text{symm} & & & G \end{bmatrix}^{(n)} \begin{Bmatrix} \varepsilon_x - \alpha T \\ \varepsilon_y - \alpha T \\ \varepsilon_z - \alpha T \\ \gamma_{xy} \end{Bmatrix}^{(n)}, \quad (8a)$$

$$\begin{Bmatrix} \tau_{yz} \\ \tau_{xz} \end{Bmatrix}^{(n)} = G^{(n)} \begin{Bmatrix} \gamma_{yz} \\ \gamma_{xz} \end{Bmatrix}^{(n)}, \quad (8b)$$

in which $E^{(n)}(z)$ and $\nu^{(n)}(z)$ are Young’s modulus and Poisson’s ratio characterizing elastic properties in the plane of isotropy of the n th layer. The shear modulus $G^{(n)}(z)$ characterizing the material response under a shear load applied in the plane of isotropy takes the form

$$G^{(n)} = \frac{E^{(n)}}{2(1 + \nu^{(n)})}. \quad (9)$$

The principle of virtual work in the present case yields

$$\int_{-h/2}^{h/2} \int_{\Omega} \left[\sigma_{xx}^{(n)} \delta \varepsilon_x + \sigma_{yy}^{(n)} \delta \varepsilon_y + \sigma_{zz}^{(n)} \delta \varepsilon_z + \tau_{xy}^{(n)} \delta \gamma_{xy} + \tau_{yz}^{(n)} \delta \gamma_{yz} + \tau_{xz}^{(n)} \delta \gamma_{xz} \right] d\Omega dz = 0, \quad (10)$$

or

$$\int_{\Omega} [N_x \delta \varepsilon_x^0 + N_{xy} \delta \gamma_{xy}^0 + N_y \delta \varepsilon_y^0 + M_x \delta k_x + M_{xy} \delta k_{xy} + M_y \delta k_y + S_x \delta \eta_x + S_{xy} \delta \eta_{xy} + S_y \delta \eta_y + N_{zz} \delta \varepsilon_z^0 + Q_{xz} \delta \gamma_{xz}^0 + Q_{yz} \delta \gamma_{yz}^0] d\Omega = 0, \tag{11}$$

where

$$\begin{Bmatrix} N_x & N_y & N_{xy} \\ M_x & M_y & M_{xy} \\ S_x & S_y & S_{xy} \end{Bmatrix} = \sum_{n=1}^3 \int_{h_{n-1}}^{h_n} (\sigma_{xx}, \sigma_{yy}, \tau_{xy})^{(n)} \begin{Bmatrix} 1 \\ z \\ \Psi(z) \end{Bmatrix} dz, \tag{12a}$$

$$N_{zz} = \sum_{n=1}^3 \int_{h_{n-1}}^{h_n} \sigma_{zz}^{(n)} \Psi''(z) dz, \tag{12b}$$

$$(Q_{xz}, Q_{yz}) = \sum_{n=1}^3 \int_{h_{n-1}}^{h_n} (\tau_{xz}, \tau_{yz})^{(n)} \Psi'(z) dz, \tag{12c}$$

where h_n and h_{n-1} are the top and bottom z -coordinates of the n th layer.

Governing equations

The governing equations of equilibrium can be derived from Eq. 11 by integrating the displacement gradients by parts and setting the coefficients δu , δv , δw , $\delta \varphi_x$, $\delta \varphi_y$, and $\delta \varphi_z$ to zero separately. Thus one can obtain the equilibrium equations associated with the present unified shear deformation theory,

$$\frac{\partial N_x}{\partial x} + \frac{\partial N_{xy}}{\partial y} = 0, \tag{13a}$$

$$\frac{\partial N_{xy}}{\partial x} + \frac{\partial N_y}{\partial y} = 0, \tag{13b}$$

$$\frac{\partial^2 M_x}{\partial x^2} + 2 \frac{\partial^2 M_{xy}}{\partial x \partial y} + \frac{\partial^2 M_y}{\partial y^2} = 0, \tag{13c}$$

$$\frac{\partial S_x}{\partial x} + \frac{\partial S_{xy}}{\partial y} - Q_{xz} = 0, \tag{13d}$$

$$\frac{\partial S_{xy}}{\partial x} + \frac{\partial S_y}{\partial y} - Q_{yz} = 0, \tag{13e}$$

$$Q_{xz,x} + Q_{yz,y} - N_{zz} = 0. \tag{13f}$$

Using Eq. 8 in Eq. 12, the stress resultants of a sandwich plate made up of three layers can be related to the total strains by

$$\begin{Bmatrix} N \\ M \\ S \end{Bmatrix} = \begin{bmatrix} A & B & B^a \\ B & D & D^a \\ B^a & D^a & F^a \end{bmatrix} \begin{Bmatrix} \varepsilon \\ \kappa \\ \eta \end{Bmatrix} + \delta_{xy} \begin{bmatrix} L \\ L^a \\ R \end{bmatrix} \varepsilon_z^0 - \begin{Bmatrix} N^T \\ M^T \\ S^T \end{Bmatrix}, Q = A^a \gamma, \tag{14}$$

$$N_{zz} = R^a \varphi_z + L(\varepsilon_x^0 + \varepsilon_y^0) + L^a(\kappa_x + \kappa_y) + R(\eta_x + \eta_y) - N_{zz}^T,$$

where δ_{xy} is the Kronecker's delta, and

$$N = \{N_x, N_y, N_{xy}\}^t, \quad M = \{M_x, M_y, M_{xy}\}^t, \tag{15a}$$

$$S = \{S_x, S_y, S_{xy}\}^t,$$

$$N^T = \{N_x^T, N_y^T, 0\}^t, \quad M^T = \{M_x^T, M_y^T, 0\}^t, \tag{15b}$$

$$S^T = \{S_x^T, S_y^T, 0\}^t,$$

$$\varepsilon = \{\varepsilon_x^0, \varepsilon_y^0, \gamma_{xy}^0\}^t, \quad \kappa = \{\kappa_x, \kappa_y, \kappa_{xy}\}^t, \quad \eta = \{\eta_x, \eta_y, \eta_{xy}\}^t, \tag{15c}$$

$$A = \begin{bmatrix} A_{11} & A_{12} & 0 \\ A_{12} & A_{22} & 0 \\ 0 & 0 & A_{66} \end{bmatrix}, \quad B = \begin{bmatrix} B_{11} & B_{12} & 0 \\ B_{12} & B_{22} & 0 \\ 0 & 0 & B_{66} \end{bmatrix}, \tag{15d}$$

$$D = \begin{bmatrix} D_{11} & D_{12} & 0 \\ D_{12} & D_{22} & 0 \\ 0 & 0 & D_{66} \end{bmatrix},$$

$$B^a = \begin{bmatrix} B_{11}^a & B_{12}^a & 0 \\ B_{12}^a & B_{22}^a & 0 \\ 0 & 0 & B_{66}^a \end{bmatrix}, \quad D^a = \begin{bmatrix} D_{11}^a & D_{12}^a & 0 \\ D_{12}^a & D_{22}^a & 0 \\ 0 & 0 & D_{66}^a \end{bmatrix}, \tag{15e}$$

$$F^a = \begin{bmatrix} F_{11}^a & F_{12}^a & 0 \\ F_{12}^a & F_{22}^a & 0 \\ 0 & 0 & F_{66}^a \end{bmatrix},$$

$$Q = \{Q_{xz}, Q_{yz}\}^t, \quad \gamma = \{\gamma_{xz}^0, \gamma_{yz}^0\}^t, \quad A^a = \begin{bmatrix} A_{44}^a & 0 \\ 0 & A_{55}^a \end{bmatrix}, \tag{15f}$$

where N and M are the basic components of stress resultants and stress couples, S are additional stress couples associated with the transverse shear effects, Q and N_{zz} are transverse and normal shear stress resultants. Note that the superscript t denotes the transpose of the given vector. The stiffness coefficients A_{ij} and B_{ij}, \dots etc., are defined as

$$\begin{Bmatrix} A_{11}, B_{11}, D_{11}, B_{11}^a, D_{11}^a, F_{11}^a \\ A_{12}, B_{12}, D_{12}, B_{12}^a, D_{12}^a, F_{12}^a \\ A_{66}, B_{66}, D_{66}, B_{66}^a, D_{66}^a, F_{66}^a \end{Bmatrix} = \sum_{n=1}^3 \int_{h_{n-1}}^{h_n} \frac{E^{(n)}}{1 - \nu^{(n)2}} (1, z, z^2, \Psi(z), z\Psi(z), \Psi^2(z)) \begin{Bmatrix} 1 \\ \nu^{(n)} \\ \frac{1 - \nu^{(n)}}{2} \end{Bmatrix} dz, \tag{16a}$$

and

$$\begin{Bmatrix} A_{22}, B_{22}, D_{22}, B_{22}^a, D_{22}^a, F_{22}^a \end{Bmatrix} = (A_{11}, B_{11}, D_{11}, B_{11}^a, D_{11}^a, F_{11}^a), \tag{16b}$$

$$\begin{Bmatrix} L \\ L^a \\ R \\ R^a \end{Bmatrix} = \sum_{n=1}^3 \int_{h_{n-1}}^{h_n} \frac{E^{(n)}}{1 - \nu^{(n)2}} \begin{Bmatrix} \nu^{(n)} \\ \nu^{(n)} z \\ \nu^{(n)} \Psi \\ \Psi'' \end{Bmatrix} \Psi'' dz, \tag{16c}$$

$$A_{44}^a = \sum_{n=1}^3 \int_{h_{n-1}}^{h_n} \frac{E^{(n)}}{2(1+\nu^{(n)})} [\Psi'(z)]^2 dz = A_{55}^a. \quad (16d)$$

The stress and moment resultants, $N_x^T = N_y^T$, $M_x^T = M_y^T$, $S_x^T = S_y^T$ and N_{zz}^T due to thermal loading are defined by

$$\begin{Bmatrix} N_x^T \\ M_x^T \\ S_x^T \\ N_{zz}^T \end{Bmatrix} = \sum_{n=1}^3 \int_{h_{n-1}}^{h_n} \frac{E^{(n)}}{1-\nu^{(n)2}} (1+2\nu^{(n)}) \alpha^{(n)} T \begin{Bmatrix} 1 \\ z \\ \Psi(z) \\ \Psi''(z) \end{Bmatrix} dz. \quad (17)$$

The temperature field variation through the thickness is assumed to be

$$T(x, y, z) = T_1(x, y) + \frac{z}{h} T_2(x, y) + \frac{\Psi(z)}{h} T_3(x, y), \quad (18)$$

where T_1 , T_2 and T_3 are thermal loads.

Substituting from Eq. 14 into Eq. 13, we obtain the following equation,

$$\begin{aligned} A_{11}d_{11}u + A_{66}d_{22}u + (A_{12} + A_{66})d_{12}v - B_{11}d_{11}w \\ - (B_{12} + 2B_{66})d_{12}w \\ + (B_{66}^a + B_{12}^a)d_{12}\varphi_y + B_{66}^a d_{22}\varphi_x \\ + B_{11}^a d_{11}\varphi_x + Ld_1\varphi_z = f_1, \end{aligned} \quad (19a)$$

$$\begin{aligned} A_{22}d_{22}v + A_{66}d_{11}v + (A_{12} + A_{66})d_{12}u - B_{22}d_{22}w \\ - (B_{12} + 2B_{66})d_{12}w \\ + (B_{66}^a + B_{12}^a)d_{12}\varphi_x + B_{66}^a d_{11}\varphi_y + B_{22}^a d_{22}\varphi_y \\ + Ld_2\varphi_z = f_2, \end{aligned} \quad (19b)$$

$$\begin{aligned} -B_{11}d_{11}u - (B_{12} + 2B_{66})d_{12}u - (B_{12} + 2B_{66})d_{12}v \\ - B_{22}d_{22}v + D_{11}d_{11}w + 2(D_{12} + 2D_{66})d_{12}w \\ + D_{22}d_{22}w - D_{11}^a d_{11}\varphi_x - (D_{12}^a + 2D_{66}^a)d_{12}\varphi_x \\ - (D_{12}^a + 2D_{66}^a)d_{12}\varphi_y - D_{22}^a d_{22}\varphi_y \\ - L^a(d_{11}\varphi_z + d_{22}\varphi_z) = f_3, \end{aligned} \quad (19c)$$

$$\begin{aligned} B_{11}^a d_{11}u + B_{66}^a d_{22}u + (B_{12}^a + B_{66}^a)d_{12}v - D_{11}^a d_{11}w \\ - (D_{12}^a + 2D_{66}^a)d_{12}w + F_{11}^a d_{11}\varphi_x + F_{66}^a d_{22}\varphi_x \\ + (F_{12}^a + F_{66}^a)d_{12}\varphi_y - A_{44}^a(\varphi_x + d_1\varphi_z) + R d_1\varphi_z \\ = f_4, \end{aligned} \quad (19d)$$

$$\begin{aligned} (B_{12}^a + B_{66}^a)d_{12}u + B_{22}^a d_{22}v + B_{66}^a d_{11}v - (D_{12}^a + 2D_{66}^a)d_{12}w \\ - D_{22}^a d_{22}w + (F_{12}^a + F_{66}^a)d_{12}\varphi_x + F_{66}^a d_{11}\varphi_y + F_{22}^a d_{22}\varphi_y \\ - A_{55}^a(\varphi_y + d_2\varphi_z) + R d_2\varphi_z = f_5, \end{aligned} \quad (19e)$$

$$\begin{aligned} L(d_{11}u + d_{22}v) - L^a(d_{11}w + d_{22}w) + (R - A_{55}^a) \\ (d_1\varphi_x + d_2\varphi_y) + R^a\varphi_z - A_{55}^a(d_{11}\varphi_z + d_{22}\varphi_z) = f_6, \end{aligned} \quad (19f)$$

where $\{f\} = \{f_1, f_2, f_3, f_4, f_5, f_6\}^t$ is a generalized force vector, d_{ij} , d_{ijl} and d_{ijlm} are the following differential operators:

$$d_{ij} = \frac{\partial^2}{\partial x_i \partial x_j}, \quad d_{ijl} = \frac{\partial^3}{\partial x_i \partial x_j \partial x_l}, \quad d_{ijlm} = \frac{\partial^4}{\partial x_i \partial x_j \partial x_l \partial x_m},$$

$$(i, j, l, m = 1, 2). \quad (20)$$

The components of the generalized force vector $\{f\}$ are given by

$$\begin{aligned} f_1 = \frac{\partial N_x^T}{\partial x}, \quad f_2 = \frac{\partial N_y^T}{\partial y}, \quad f_3 = -\frac{\partial^2 M_x^T}{\partial x^2} - \frac{\partial^2 M_y^T}{\partial y^2}, \\ f_4 = \frac{\partial S_x^T}{\partial x}, \quad f_5 = \frac{\partial S_y^T}{\partial y}, \quad f_6 = N_{zz}^T. \end{aligned} \quad (21)$$

For further computational reasons the converted expressions of the stress components are also recorded. They read

$$\begin{aligned} \sigma_{xx}^{(n)} = \frac{E^{(n)}}{1-\nu^{(n)2}} \left\{ \frac{\partial u}{\partial x} + \nu^{(n)} \frac{\partial v}{\partial y} - z \left(\frac{\partial^2 w}{\partial x^2} + \nu^{(n)} \frac{\partial^2 w}{\partial y^2} \right) \right. \\ \left. + \Psi(z)(\varphi_{x,x} + \nu^{(n)}\varphi_{y,y}) + \nu^{(n)}\Psi''(z)\varphi_z \right. \\ \left. - (1+2\nu^{(n)})\alpha^{(n)}T \right\}, \end{aligned} \quad (22a)$$

$$\begin{aligned} \sigma_{yy}^{(n)} = \frac{E^{(n)}}{1-\nu^{(n)2}} \left\{ \nu^{(n)} \frac{\partial u}{\partial x} + \frac{\partial v}{\partial y} - z \left(\nu^{(n)} \frac{\partial^2 w}{\partial x^2} + \frac{\partial^2 w}{\partial y^2} \right) \right. \\ \left. + \Psi(z)(\varphi_{y,y} + \nu^{(n)}\varphi_{x,x}) \right. \\ \left. + \nu^{(n)}\Psi''(z)\varphi_z - (1+2\nu^{(n)})\alpha^{(n)}T \right\}, \end{aligned} \quad (22b)$$

$$\begin{aligned} \sigma_{zz}^{(n)} = \frac{E^{(n)}}{1-\nu^{(n)2}} \left\{ \nu^{(n)} \left(\frac{\partial u}{\partial x} + \frac{\partial v}{\partial y} \right) - z\nu^{(n)} \left(\frac{\partial^2 w}{\partial x^2} + \frac{\partial^2 w}{\partial y^2} \right) \right. \\ \left. + \Psi(z)\nu^{(n)}(\varphi_{x,x} + \varphi_{y,y}) + \Psi''(z)\varphi_z - (1+2\nu^{(n)})\alpha^{(n)}T \right\}, \end{aligned} \quad (22c)$$

$$\begin{aligned} \tau_{xy}^{(n)} = \frac{E^{(n)}}{2(1+\nu^{(n)})} \left\{ \frac{\partial u}{\partial y} + \frac{\partial v}{\partial x} - 2z \frac{\partial^2 w}{\partial x \partial y} + \Psi(z)(\varphi_{x,y} + \varphi_{y,x}) \right\}, \end{aligned} \quad (22d)$$

$$\tau_{yz}^{(n)} = \frac{E^{(n)}}{2(1+\nu^{(n)})} \Psi'(z) \left(\varphi_y + \frac{\partial \varphi_z}{\partial y} \right), \quad (22e)$$

$$\tau_{xz}^{(n)} = \frac{E^{(n)}}{2(1+\nu^{(n)})} \Psi'(z) \left(\varphi_x + \frac{\partial \varphi_z}{\partial x} \right). \quad (22f)$$

Exact solution for a simply-supported FGM sandwich plate

Rectangular plates are generally classified in accordance with the type of support used. We are here concerned with the exact solution of Eqs. (19a–f) for a simply supported FGM plate. The following boundary conditions are imposed at the side edges for SSDPT:

$$\begin{aligned} v = w = \varphi_y = \varphi_z = N_x = M_x = S_x = 0 \quad \text{at } x = 0, a \\ u = w = \varphi_x = \varphi_z = N_y = M_y = S_y = 0 \quad \text{at } y = 0, b \end{aligned} \tag{23a}$$

For TSDPT and FSDPT, the boundary conditions are

$$\begin{aligned} v = w = \varphi_y = N_x = M_x = S_x = 0 \quad \text{at } x = 0, a \\ u = w = \varphi_x = N_y = M_y = S_y = 0 \quad \text{at } y = 0, b \end{aligned} \tag{23b}$$

For CLPT, the boundary conditions are

$$\begin{aligned} v = w = N_x = M_x = 0 \quad \text{at } x = 0, a \\ u = w = N_y = M_y = 0 \quad \text{at } y = 0, b \end{aligned} \tag{23c}$$

To solve this problem, Navier presented the transverse temperature loads $T_1, T_2,$ and T_3 in the form of a double trigonometric series as

$$\begin{Bmatrix} T_1 \\ T_2 \\ T_3 \end{Bmatrix} = \begin{Bmatrix} \bar{T}_1 \\ \bar{T}_2 \\ \bar{T}_3 \end{Bmatrix} \sin(\lambda x) \sin(\mu y), \tag{24}$$

where $\lambda = \pi/a, \mu = \pi/b, \bar{T}_1, \bar{T}_2,$ and \bar{T}_3 are constants. Following the Navier solution procedure, we assume the following solution form for $u, v, w, \varphi_x, \varphi_y$ and φ_z that satisfies the boundary conditions,

$$\begin{Bmatrix} u \\ v \\ w \\ \varphi_x \\ \varphi_y \\ \varphi_z \end{Bmatrix} = \begin{Bmatrix} U \cos(\lambda x) \sin(\mu y) \\ V \sin(\lambda x) \cos(\mu y) \\ W \sin(\lambda x) \sin(\mu y) \\ X \cos(\lambda x) \sin(\mu y) \\ Y \sin(\lambda x) \cos(\mu y) \\ Z \sin(\lambda x) \sin(\mu y) \end{Bmatrix}, \tag{25}$$

where $U, V, W, X, Y,$ and Z are arbitrary parameters to be determined subjected to the condition that the solution in Eq. 25 satisfies governing equations (19). One obtains the following operator equation,

$$[C]\{\Delta\} = \{F\}, \tag{26}$$

where $\{\Delta\} = \{U, V, W, X, Y, Z\}^t,$ and $[C]$ is the symmetric matrix given by

$$\begin{aligned} C_{11} &= -(A_{11}\lambda^2 + A_{66}\mu^2), \\ C_{12} &= -\lambda\mu(A_{12} + A_{66}), \\ C_{13} &= \lambda[B_{11}\lambda^2 + (B_{12} + 2B_{66})\mu^2], \\ C_{14} &= -(B_{11}^a\lambda^2 + B_{66}^a\mu^2), \\ C_{15} &= -(B_{12}^a + B_{66}^a)\lambda\mu, \\ C_{16} &= \lambda L, \\ C_{22} &= -(A_{66}\lambda^2 + A_{22}\mu^2), \\ C_{23} &= \mu[(B_{12} + 2B_{66})\lambda^2 + B_{22}\mu^2], \\ C_{24} &= C_{15}, \end{aligned}$$

$$\begin{aligned} C_{25} &= -(B_{66}^a\lambda^2 + B_{22}^a\mu^2), \\ C_{26} &= \mu L, \\ C_{33} &= -[D_{11}\lambda^4 + 2(D_{12} + 2D_{66})\lambda^2\mu^2 + D_{22}\mu^4], \\ C_{34} &= \lambda[D_{11}^a\lambda^2 + (D_{12}^a + 2D_{66}^a)\mu^2], \\ C_{35} &= \mu[(D_{12}^a + 2D_{66}^a)\lambda^2 + D_{22}^a\mu^2], \\ C_{36} &= -L^a(\lambda^2 + \mu^2), \\ C_{44} &= -[F_{11}^a\lambda^2 + F_{66}^a\mu^2 + A_{44}^a], \\ C_{45} &= -\lambda\mu(F_{12}^a + F_{66}^a), \\ C_{46} &= \lambda(R - A_{44}^a), \\ C_{55} &= -[F_{66}^a\lambda^2 + F_{22}^a\mu^2 + A_{55}^a], \\ C_{56} &= \mu(R - A_{55}^a), \\ C_{66} &= \lambda^2 A_{44}^a + \mu^2 A_{55}^a + R^a. \end{aligned} \tag{27}$$

The components of the generalized force vector $\{F\} = \{F_1, F_2, F_3, F_4, F_5, F_6\}^t$ are given by

$$\begin{aligned} F_1 &= \lambda(A^T \bar{T}_1 + B^T \bar{T}_2 + {}^a B^T \bar{T}_3), \\ F_2 &= \mu(A^T \bar{T}_1 + B^T \bar{T}_2 + {}^a B^T \bar{T}_3), \\ F_3 &= -h(\lambda^2 + \mu^2)[B^T \bar{T}_1 + D^T \bar{T}_2 + {}^a D^T \bar{T}_3], \\ F_4 &= \lambda h({}^a B^T \bar{T}_1 + {}^a D^T \bar{T}_2 + {}^a F^T \bar{T}_3), \\ F_5 &= \mu h({}^a B^T \bar{T}_1 + {}^a D^T \bar{T}_2 + {}^a F^T \bar{T}_3), \\ F_6 &= h(L^T \bar{T}_1 + {}^a L^T \bar{T}_2 + R^T \bar{T}_3), \end{aligned} \tag{28}$$

where

$$\{A^T, B^T, D^T\} = \sum_{n=1}^3 \int_{h_{n-1}}^{h_n} \frac{E^{(n)}}{1 - [v^{(n)}]^2} (1 + 2v^{(n)}) \alpha^{(n)} \{1, \bar{z}, \bar{z}^2\} dz, \tag{29a}$$

$$\{{}^a B^T, {}^a D^T, {}^a F^T\} = \sum_{n=1}^3 \int_{h_{n-1}}^{h_n} \frac{E^{(n)}}{1 - [v^{(n)}]^2} (1 + 2v^{(n)}) \alpha^{(n)} \bar{\Psi}(z) \{1, \bar{z}, \bar{\Psi}(z)\} dz, \tag{29b}$$

$$\{L^T, {}^a L^T, R^T\} = \sum_{n=1}^3 \int_{h_{n-1}}^{h_n} \frac{E^{(n)}}{1 - [v^{(n)}]^2} (1 + 2v^{(n)}) \alpha^{(n)} \bar{\Psi}''(z) \{1, \bar{z}, \bar{\Psi}(z)\} dz, \tag{29c}$$

in which $\bar{z} = \frac{z}{h}, \bar{\Psi}(z) = \frac{\Psi(z)}{h}$ and $\bar{\Psi}''(z) = \frac{\Psi''(z)}{h}$.

Also, the stress components are recorded. They read

$$\begin{aligned} \sigma_{xx}^{(n)} &= \frac{E^{(n)}}{1 - v^{(n)}} \left\{ -(\lambda U + v^{(n)} \mu V) + z(\lambda^2 + v^{(n)} \mu^2) W \right. \\ &\quad \left. - \Psi(z)(\lambda X + v^{(n)} \mu Y) + v^{(n)} \Psi''(z) Z - (1 + 2v^{(n)}) \alpha^{(n)} \right. \\ &\quad \left. (\bar{T}_1 + \bar{z} \bar{T}_2 + \bar{\Psi} \bar{T}_3) \right\} \sin(\lambda x) \sin(\mu y), \end{aligned} \tag{30a}$$

$$\sigma_{yy}^{(n)} = \frac{E^{(n)}}{1 - \nu^{(n)2}} \left\{ -(\nu^{(n)}\lambda U + \mu V) + z(\nu^{(n)}\lambda^2 + \mu^2)W - \Psi(z)(\nu^{(n)}\lambda X + \mu Y) + \nu^{(n)}\Psi''(z)Z - (1 + 2\nu^{(n)})\alpha^{(n)}(\bar{T}_1 + \bar{z}\bar{T}_2 + \bar{\Psi}\bar{T}_3) \right\} \sin(\lambda x) \sin(\mu y), \tag{30b}$$

$$\sigma_{zz}^{(n)} = \frac{E^{(n)}}{1 - \nu^{(n)2}} \left\{ -\nu^{(n)}(\lambda U + \mu V) + z\nu^{(n)}(\lambda^2 + \mu^2)W - \nu^{(n)}\Psi(z)(\lambda X + \mu Y) + \Psi''(z)Z - (1 + 2\nu^{(n)})\alpha^{(n)}(\bar{T}_1 + \bar{z}\bar{T}_2 + \bar{\Psi}\bar{T}_3) \right\} \sin(\lambda x) \sin(\mu y), \tag{30c}$$

$$\tau_{xy}^{(n)} = \frac{E^{(n)}}{2(1 + \nu^{(n)})} \left\{ \mu U + \lambda V - 2z\lambda\mu W + \Psi(z)(\mu X + \lambda Y) \right\} \cos(\lambda x) \cos(\mu y), \tag{30d}$$

$$\tau_{yz}^{(n)} = \frac{E^{(n)}}{2(1 + \nu^{(n)})} \Psi'(z) (Y + \mu Z) \sin(\lambda x) \cos(\mu y), \tag{30e}$$

$$\tau_{xz}^{(n)} = \frac{E^{(n)}}{2(1 + \nu^{(n)})} \Psi'(z) (X + \lambda Z) \cos(\lambda x) \sin(\mu y). \tag{30f}$$

Several kinds of sandwich plates

Figure 2 shows the through-the-thickness variation of the volume fraction function of the ceramic for $k = 0.01, 0.1, 0.5, 1.5,$ and 5 . Note that the core of the plate is fully ceramic while the bottom and top surfaces of the plate are metal-rich.

The (1-0-1) FGM sandwich plate

As shown in Fig. 2a, the plate is symmetric and made of only two equal-thickness FGM layers, i.e. there is no core layer. Thus,

$$h_1 = h_2 = 0. \tag{31}$$

The (1-1-1) FGM sandwich plate

Here the plate is symmetric and made of three equal-thickness layers (see Fig. 2b). In this case, we have

$$h_1 = -h/6, \quad h_2 = h/6. \tag{32}$$

The (1-2-1) FGM sandwich plate

As shown in Fig. 2c, the plate is symmetric, in which the core thickness equals the sum of faces thickness. So, one obtain

$$h_1 = -h/4, \quad h_2 = h/4. \tag{33}$$

The (2-1-2) FGM sandwich plate

Here the plate is also symmetric and the thickness of the core is half the face thickness. Figure 2d shows that

$$h_1 = -h/10, \quad h_2 = h/10. \tag{34}$$

The (2-2-1) FGM sandwich plate

In this case the plate is not symmetric and the core thickness is the same as one face while it is twice the other (see Fig. 2e). Thus

$$h_1 = -h/10, \quad h_2 = 3h/10. \tag{35}$$

Numerical results

The static analysis is conducted for combinations of metal and ceramic. The set of materials chosen is Titanium and Zirconia. For simplicity, Poisson’s ratio of the two materials is assigned the same value. So, Young’s modulus and thermal expansion coefficient are written as the following:

Metal: Ti–6Al–4V	Ceramic: ZrO ₂
$E_m = 66.2$ GPa	$E_c = 117.0$ GPa
$\nu = 1/3$	$\nu = 1/3$
$\alpha_m = 10.3 \times (10^{-6}/K)$	$\alpha_c = 7.11 \times (10^{-6}/K)$

To illustrate the preceding thermal–structural analysis, a variety of sample problems is considered. For the sake of brevity, only linearly varying (across the thickness) temperature distribution $T = \bar{z}T_2$, non-linearly varying (across the thickness) temperature distribution $T = \bar{\Psi}(z)T_3$, and a combination of both $T = \bar{z}T_2 + \bar{\Psi}(z)T_3$ are considered. Note that, in most of the literature, the thermal stress problems are treated under a steady state temperature distribution that is linear with respect to the thickness direction.

Different dimensionless quantities are used for pure temperature loading as:

$$\text{center deflection } \bar{w} = \frac{h}{\alpha_0 \bar{T}_2 a^2} w \left(\frac{a}{2}, \frac{b}{2} \right),$$

$$\text{axial stress } \bar{\sigma}_{xx} = \frac{h^2}{\alpha_0 \bar{T}_2 E_0 a^2} \sigma_{xx} \left(\frac{a}{2}, \frac{b}{2}, \frac{h}{2} \right),$$

$$\text{shear stress } \bar{\tau}_{xz} = \frac{10h}{\alpha_0 \bar{T}_2 E_0 a} \tau_{xz} \left(0, \frac{b}{2}, 0 \right),$$

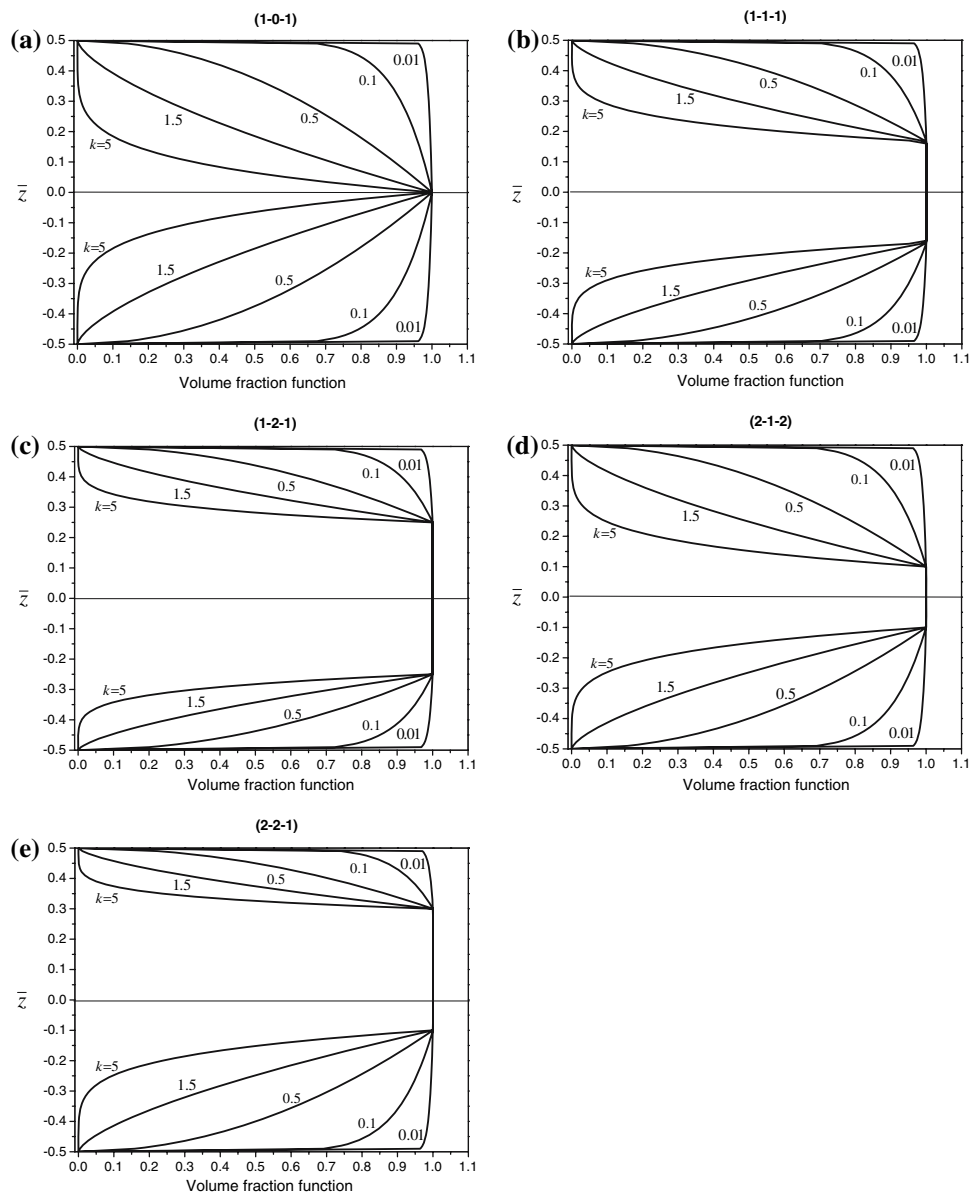


Fig. 2 Variation of volume fraction function through plate thickness for various values of the power-law index k and different types of sandwich plates: (a) The (1-0-1) FGM sandwich plate, (b) the

(1-1-1) FGM sandwich plate, (c) the (1-2-1) FGM sandwich plate, (d) the (2-1-2) FGM sandwich plate, and (e) the (2-2-1) FGM sandwich plate

where the reference values are taken as $E_0 = 1$ GPa and $\alpha_0 = 10^{-6}/K$. Numerical results are tabulated in Tables 1–4 using different plate theories. Additional results are plotted in Figs. 3–8 using the present sinusoidal shear deformation plate theory (SSDPT) with $\varphi_z \neq 0$. The effect of transverse normal and shear deformations are both included. It is assumed, unless otherwise stated, that $al/h = 10$, $a/b = 1$, $\bar{T}_1 = 0$ and $\bar{T}_2 = 100$. The shear correction factor of FSDPT is fixed to be $K = 5/6$.

Table 1 contains the dimensionless center deflection \bar{w} for an FGM sandwich plate subjected to thermal field varying linearly through the thickness ($\bar{T}_3 = 0$). The

deflections are considered for $k = 0, 1, 2, 3, 4$, and 5 and different types of sandwich plates. Table 1 shows that the effect of both shear and normal deformations is to decrease the deflections. However, the difference between shear deformation theories is less significant when $\varphi_z = 0$ especially for fully ceramic plates ($k = 0$).

Table 2 compares the deflections of different types of the FGM rectangular sandwich plates with $k = 3$. The deflections decrease as the aspect ratio a/b increases and this irrespective of the type of the sandwich plate. The inclusion of the normal deformation will decrease the deflections.

Table 1 Dimensionless center deflections \bar{w} of the different sandwich square plates ($\bar{T}_3 = 0$)

k	Theory ^a	\bar{w}				
		1-0-1	1-1-1	1-2-1	2-1-2	2-2-1
0	SSDPT	0.461634 (0.480262)	0.461634 (0.480262)	0.461634 (0.480262)	0.461634 (0.480262)	0.461634 (0.480262)
	TSDPT	0.480262	0.480262	0.480262	0.480262	0.480262
	FSDPT	0.480262	0.480262	0.480262	0.480262	0.480262
1	SSDPT	0.614565 (0.636916)	0.586124 (0.606292)	0.563416 (0.582343)	0.599933 (0.621098)	0.573327 (0.592604)
	TSDPT	0.636891	0.606256	0.582302	0.621067	0.592568
	FSDPT	0.636667	0.605936	0.581932	0.620792	0.592239
2	SSDPT	0.647135 (0.671503)	0.618046 (0.639361)	0.590491 (0.609875)	0.633340 (0.656142)	0.601843 (0.621581)
	TSDPT	0.671486	0.639325	0.609829	0.656115	0.621544
	FSDPT	0.671339	0.639028	0.609438	0.655893	0.621215
3	SSDPT	0.658153 (0.683572)	0.631600 (0.653671)	0.602744 (0.622467)	0.646475 (0.670275)	0.614121 (0.634175)
	TSDPT	0.683560	0.653638	0.622420	0.670253	0.634139
	FSDPT	0.683467	0.653374	0.622035	0.670077	0.633826
4	SSDPT	0.662811 (0.688803)	0.638705 (0.661291)	0.609560 (0.629533)	0.652890 (0.677321)	0.620663 (0.640940)
	TSDPT	0.688795	0.661260	0.629487	0.677303	0.640905
	FSDPT	0.688734	0.661022	0.629112	0.677160	0.640607
5	SSDPT	0.665096 (0.691420)	0.642948 (0.665898)	0.613842 (0.634003)	0.656490 (0.681343)	0.624629 (0.645070)
	TSDPT	0.691415	0.665869	0.633958	0.681327	0.645036
	FSDPT	0.691373	0.665649	0.633591	0.681207	0.644749

^a Number in parenthesis based on the present theory without normal deformation

Table 2 Effect of aspect ratio ab on the dimensionless deflection of the FGM sandwich plates ($k = 3, \bar{T}_3 = 0$)

Scheme	Theory ^a	\bar{w}				
		$ab = 1$	$ab = 2$	$ab = 3$	$ab = 4$	$ab = 5$
1-0-1	SSDPT	0.658153 (0.683572)	0.270902 (0.273492)	0.141810 (0.136798)	0.088642 (0.080512)	0.062334 (0.052678)
	TSDPT	0.683560	0.273480	0.136786	0.080501	0.052667
	FSDPT	0.683467	0.273387	0.136693	0.080408	0.052574
1-1-1	SSDPT	0.631600 (0.653671)	0.259980 (0.261647)	0.136105 (0.130971)	0.085094 (0.077163)	0.059862 (0.050554)
	TSDPT	0.653638	0.261614	0.130939	0.077131	0.050522
	FSDPT	0.653374	0.261350	0.130675	0.076868	0.050260
1-2-1	SSDPT	0.602744 (0.622467)	0.248135 (0.249245)	0.129933 (0.124837)	0.081262 (0.073610)	0.057192 (0.048277)
	TSDPT	0.622420	0.249199	0.124791	0.073564	0.048231
	FSDPT	0.622035	0.248814	0.124407	0.073181	0.047849
2-1-2	SSDPT	0.646475 (0.670275)	0.266094 (0.268228)	0.139295 (0.134212)	0.087077 (0.079029)	0.061244 (0.051740)
	TSDPT	0.670253	0.268206	0.134190	0.079007	0.051718
	FSDPT	0.670077	0.268031	0.134015	0.078833	0.051544
2-2-1	SSDPT	0.614121 (0.634175)	0.252758 (0.253878)	0.132303 (0.127113)	0.082701 (0.074914)	0.058168 (0.049101)
	TSDPT	0.634139	0.253843	0.127077	0.074879	0.049066
	FSDPT	0.633826	0.253531	0.126765	0.074568	0.048756

^a Number in parenthesis based on the present theory without normal deformation

Table 3 lists values of axial stress $\bar{\sigma}_{xx}$ for $k = 0, 1, 2, 3, 4$, and 5 and different types of sandwich plates. Once again, the plate is subjected to a thermal field varying

linearly through its thickness. All theories (FSDPT, TSDPT, and SSDPT with $\varphi_z = 0$) give the same axial stress $\bar{\sigma}_{xx}$ for a fully ceramic plate ($k = 0$). Once again,

Table 3 Dimensionless axial stresses $\bar{\sigma}_{xx}$ of the FGM sandwich square plates ($\bar{T}_3 = 0$)

<i>k</i>	Theory ^a	$\bar{\sigma}_{xx}$				
		1-0-1	1-1-1	1-2-1	2-1-2	2-2-1
0	SSDPT	-2.286893 (-2.079675)	-2.286893 (-2.079675)	-2.286893 (-2.079675)	-2.286893 (-2.079675)	-2.286893 (-2.079675)
	TSDPT	-2.079675	-2.079675	-2.079675	-2.079675	-2.079675
	FSDPT	-2.079675	-2.079675	-2.079675	-2.079675	-2.079675
1	SSDPT	-2.277311 (-1.993885)	-2.482321 (-2.144369)	-2.639491 (-2.261939)	-2.383671 (-2.071622)	-2.653105 (-2.276155)
	TSDPT	-1.993921	-2.144422	-2.262000	-2.071668	-2.276209
	FSDPT	-1.994116	-2.144707	-2.262332	-2.071911	-2.276503
2	SSDPT	-2.047272 (-1.824065)	-2.268798 (-1.982233)	-2.465763 (-2.127124)	-2.154066 (-1.899672)	-2.492766 (-2.152815)
	TSDPT	-1.824089	-1.982285	-2.127193	-1.899711	-2.152872
	FSDPT	-1.824214	-1.982549	-2.127548	-1.899905	-2.153170
3	SSDPT	-1.963621 (-1.764689)	-2.173723 (-1.911970)	-2.384720 (-2.065398)	-2.058212 (-1.830216)	-2.421808 (-2.099241)
	TSDPT	-1.764705	-1.912017	-2.065467	-1.830246	-2.099296
	FSDPT	-1.764783	-1.912249	-2.065816	-1.830397	-2.099579
4	SSDPT	-1.926265 (-1.738915)	-2.122027 (-1.874521)	-2.338550 (-2.030732)	-2.009198 (-1.795543)	-2.383070 (-2.070371)
	TSDPT	-1.738925	-1.874564	-2.030800	-1.795568	-2.070424
	FSDPT	-1.738976	-1.874773	-2.031140	-1.795690	-2.070694
5	SSDPT	-1.907167 (-1.726003)	-2.090296 (-1.851867)	-2.309021 (-2.008794)	-1.980712 (-1.775738)	-2.359110 (-2.052671)
	TSDPT	-1.726010	-1.851906	-2.008861	-1.775759	-2.052722
	FSDPT	-1.726045	-1.852097	-2.009191	-1.775861	-2.052982

^a Number in parenthesis based on the present theory without normal deformation

Table 4 Dimensionless transverse shear stresses $\bar{\tau}_{xz}$ of the FGM sandwich square plates ($\bar{T}_3 = -100$)

<i>k</i>	Theory ^a	$\bar{\tau}_{xz}$				
		1-0-1	1-1-1	1-2-1	2-1-2	2-2-1
0	SSDPT	0.762438 (0.574063)	0.762438 (0.574063)	0.762438 (0.574063)	0.762438 (0.574063)	0.762438 (0.574063)
	TSDPT	0.466349	0.466349	0.466349	0.466349	0.466349
1	SSDPT	0.916983 (0.696774)	0.911165 (0.694817)	0.922812 (0.705270)	0.905127 (0.689077)	0.914313 (0.697901)
	TSDPT	0.564059	0.559957	0.566925	0.556662	0.562231
2	SSDPT	0.919218 (0.696044)	0.905787 (0.689620)	0.930546 (0.711266)	0.894489 (0.679194)	0.916889 (0.699571)
	TSDPT	0.565881	0.556769	0.571546	0.550567	0.564062
3	SSDPT	0.923419 (0.697635)	0.896673 (0.681516)	0.930393 (0.710627)	0.883314 (0.669256)	0.914156 (0.696850)
	TSDPT	0.568711	0.551237	0.571319	0.544027	0.562514
4	SSDPT	0.931204 (0.702617)	0.888770 (0.674664)	0.928612 (0.708782)	0.875373 (0.662291)	0.911369 (0.694226)
	TSDPT	0.573624	0.546464	0.570117	0.539446	0.560893
5	SSDPT	0.940770 (0.709315)	0.882525 (0.669326)	0.926543 (0.706815)	0.870190 (0.657748)	0.909225 (0.692229)
	TSDPT	0.579531	0.542724	0.568771	0.536526	0.559642

^a Number in parenthesis based on the present theory without normal deformation

the inclusion of the normal deformation gives axial stresses less than those obtained from other shear deformation theories. In general, the axial stress increases as *k* increases.

Table 4 shows similar results of transverse shear stress $\bar{\tau}_{xz}$ for FGM sandwich plate subjected to a combination of

linearly and non-linearly thermal field ($\bar{T}_3 = -100$). The relative difference between SSDPT (with and without normal deformation) and TSDPT may be stable for different values of *k* and this irrespective of the type of the FGM sandwich plate. The transverse shear stress decreases for *k* ≥ 2 except in the case of the (1-0-1) FGM sandwich plate.

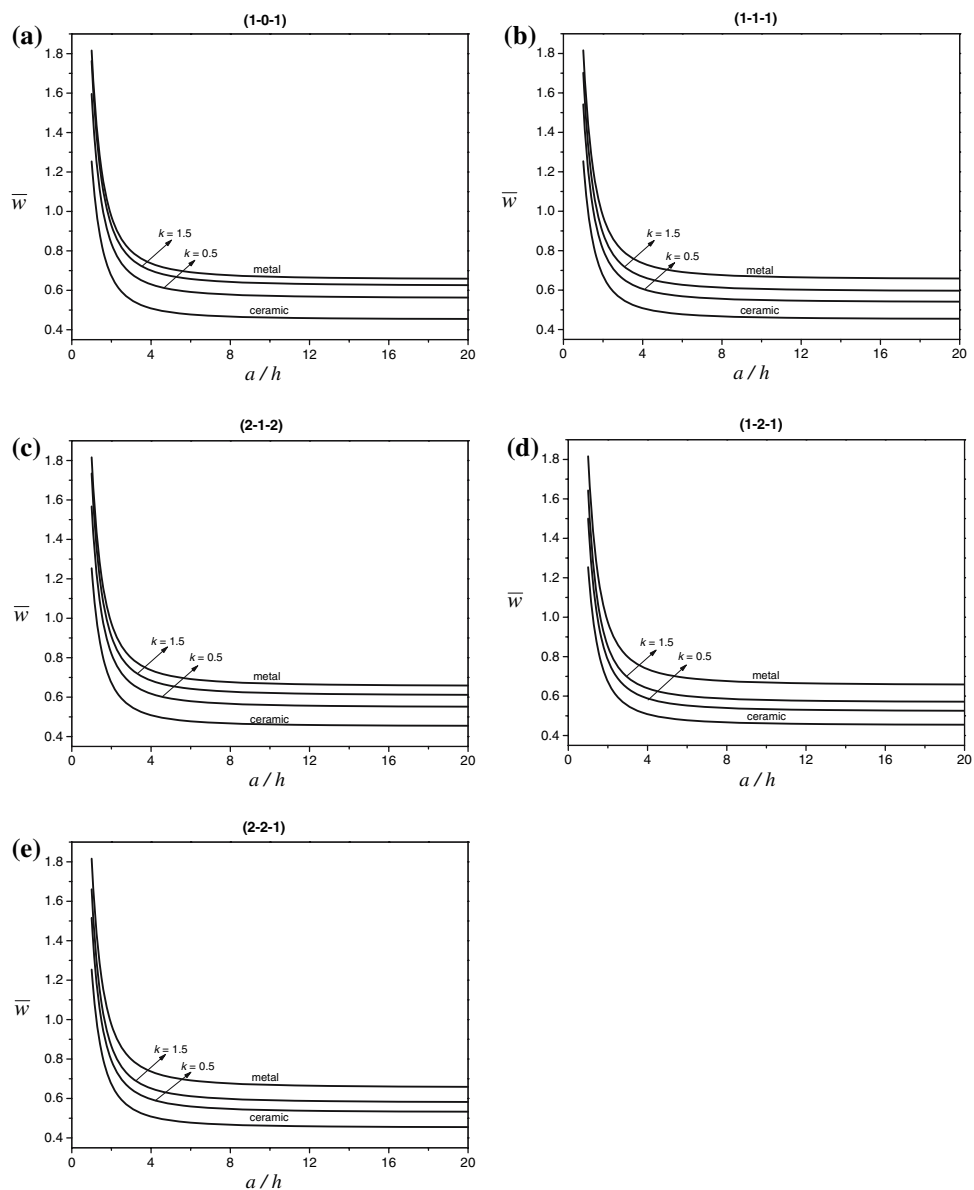


Fig. 3 Dimensionless center deflection \bar{w} as a function of side-to-thickness ratio a/h for different types of sandwich plates: **(a)** The (1-0-1) FGM sandwich plate, **(b)** the (1-1-1) FGM sandwich plate,

(c) the (1-2-1) FGM sandwich plate, **(d)** the (2-1-2) FGM sandwich plate, and **(e)** the (2-2-1) FGM sandwich plate

It is to be noted that the CLPT yields identical center deflections and axial stresses with the FSDPT and so Tables 1–3 lack the results of CLPT. In addition, the transverse shear stresses as per the FSDPT are indistinguishable and so Table 4 lacks the results of FSDPT. In general, the fully ceramic plates give the smallest deflections, transverse shear stresses. As the volume fraction exponent increases for FG plates, the deflection and axial stress will increase. In fact the non-symmetric (2-2-1) FGM plate yields the smallest axial stresses. But the symmetric (2-1-2) FGM plate yields the smallest transverse shear stresses.

Figure 3 shows the variation of the center deflection \bar{w} with side-to-thickness ratio a/h for different types of sandwich plates. The deflection of the metallic plate is found to be the largest magnitude and that of the ceramic plate of the smallest magnitude. The deflections of the FGM sandwich plates decreases as a/h increases and may be unchanged for $a/h > 5$. It is to be noted that the FGM sandwich plates with intermediate properties undergo corresponding intermediate values of center deflection. This is expected because the metallic plate is the one with the lowest stiffness and the ceramic plate is the one with the highest stiffness.

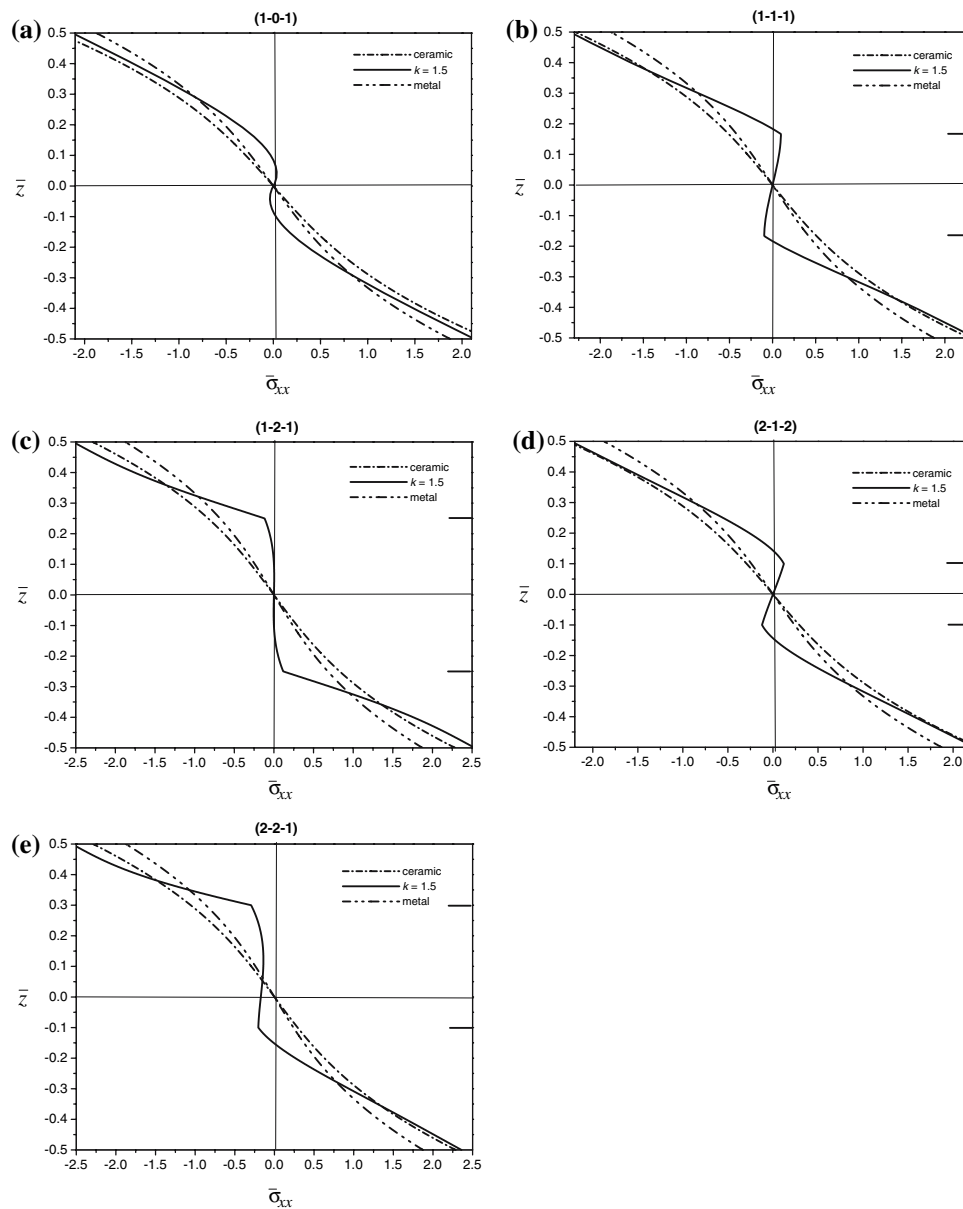


Fig. 4 Variation of axial stress $\bar{\sigma}_{xx}$ through the plate thickness for different types of sandwich plates: **(a)** The (1-0-1) FGM sandwich plate, **(b)** the (1-1-1) FGM sandwich plate, **(c)** the (1-2-1) FGM

sandwich plate, **(d)** the (2-1-2) FGM sandwich plate, and **(e)** the (2-2-1) FGM sandwich plate

Figure 4 contains the plots of the axial stress $\bar{\sigma}_{xx}$ through-the-thickness of the ceramic, FGM ($k = 1.5$), and metal plates. The stresses are tensile below the mid-plane and compressive above the mid-plane except for the non-symmetric (2-2-1) FGM plate. The axial stress is continuous through the plate thickness. Figure 4c shows that the (1-2-1) FGM plate yields the maximum tensile {minimum compressive} stress at the bottom {top} surface of the plate. These surfaces are metal-rich for the FGM plate. However, the (2-2-1) FGM plate yields the minimum compressive stress at the top surface of the

plate (see Fig. 4e). In addition, all types of FGM plate yield the maximum compressive {minimum tensile} stress at the top {bottom} surface of the core layer. These are the ceramic-rich surfaces in which the ceramic plate experiences the minimum compressive or maximum tensile stresses.

In Fig. 5 we have plotted the through-the-thickness distributions of the transverse shear stress $\bar{\tau}_{xz}$. The maximum value occurs at a point on the mid-plane of the plate and its magnitude for FGM plate is larger than that for homogeneous plates.

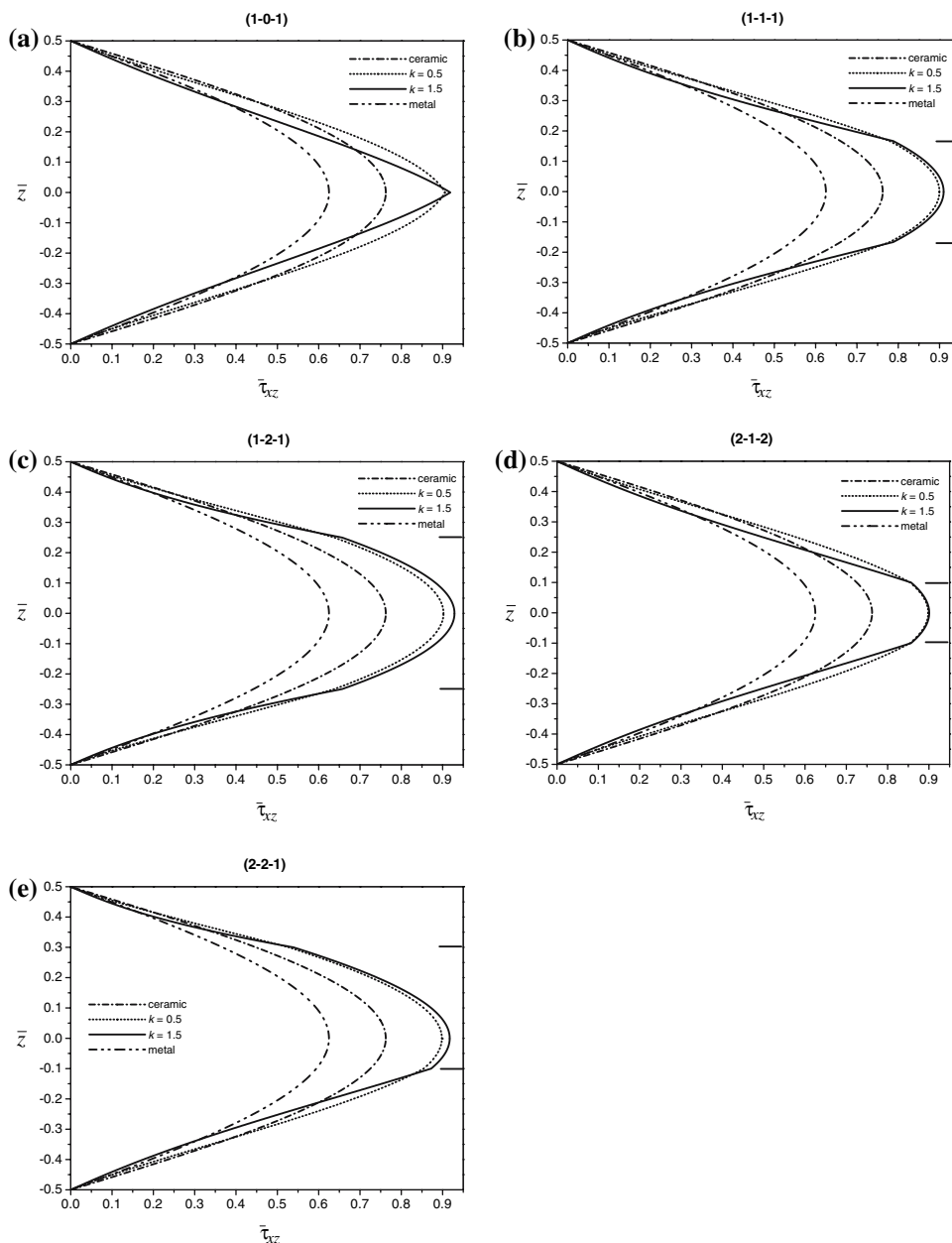


Fig. 5 Variation of transverse shear stress $\bar{\tau}_{xz}$ through the plate thickness for different types of FGM sandwich plates: **(a)** The (1-0-1) FGM sandwich plate, **(b)** the (1-1-1) FGM sandwich plate, **(c)** the

(1-2-1) FGM sandwich plate, **(d)** the (2-1-2) FGM sandwich plate, and **(e)** the (2-2-1) FGM sandwich plate

Figure 6 shows the effects of the aspect ratio ab on the dimensionless deflection \bar{w} . The deflection decreases as ab increases. The deflection of the metallic plate is found to be the largest magnitude and that of the ceramic plate, of the smallest magnitude. It is to be noted that the FGM sandwich plate with intermediate properties undergo corresponding intermediate values of center deflection.

Now, we will turn our attention to the effect of thermal load \bar{T}_3 on the deflection and stresses. Figure 7 shows the effects of the side-to-thickness ratio alh and the aspect ratio ab on the dimensionless center deflection \bar{w} for FGM plates ($k = 0.5$) subjected to nonlinearly distributed temperature field. It is found that the side-to-thickness ratio effect and the aspect ratio effect are more pronounced on the thermal bending deflection \bar{w} of a plate under uniform

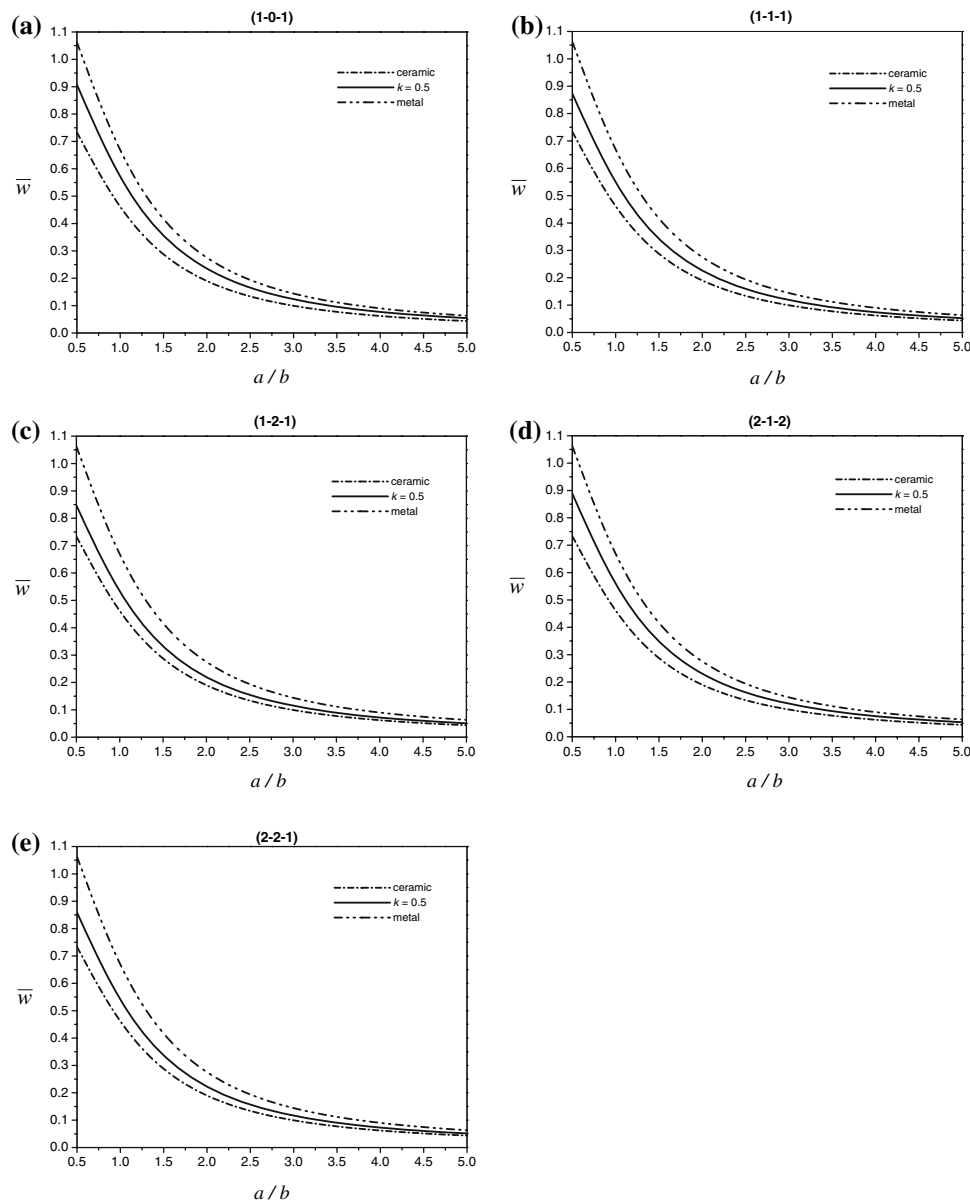


Fig. 6 Effect of the aspect ratio a/b on the dimensionless center deflection \bar{w} of different types of FGM sandwich plates: **(a)** The (1-0-1) FGM sandwich plate, **(b)** the (1-1-1) FGM sandwich plate,

(c) the (1-2-1) FGM sandwich plate, **(d)** the (2-1-2) FGM sandwich plate, and **(e)** the (2-2-1) FGM sandwich plate

temperature distribution $\bar{T}_3 = 100$, and it is less pronounced on the non-uniform thermal plate $\bar{T}_3 = -100$. But when $\bar{T}_3 = 0$, the center deflection takes intermediate values between non-uniform and uniform thermal plate.

In Fig. 8 we have plotted the through-the-thickness distributions of the dimensionless axial stress $\bar{\sigma}_{xx}$ and the transverse shear stress $\bar{\tau}_{xz}$ through-the-thickness of the (1-1-1) FGM plate ($k = 1.5$). Figure 8 reveals that the variation of stresses is very sensitive to the variation of the thermal load \bar{T}_3 value.

Conclusion

The purpose of this article is to develop the bending behavior of the three layer sandwich plates, which are constructed in such a manner that those assumptions stated previously are satisfied, due to a general type of externally applied thermal load. The shear theories of sandwich plates are used to investigate the bending response under a sinusoidal distribution of temperature field. The effect of transverse normal strain as well as the effect of shear

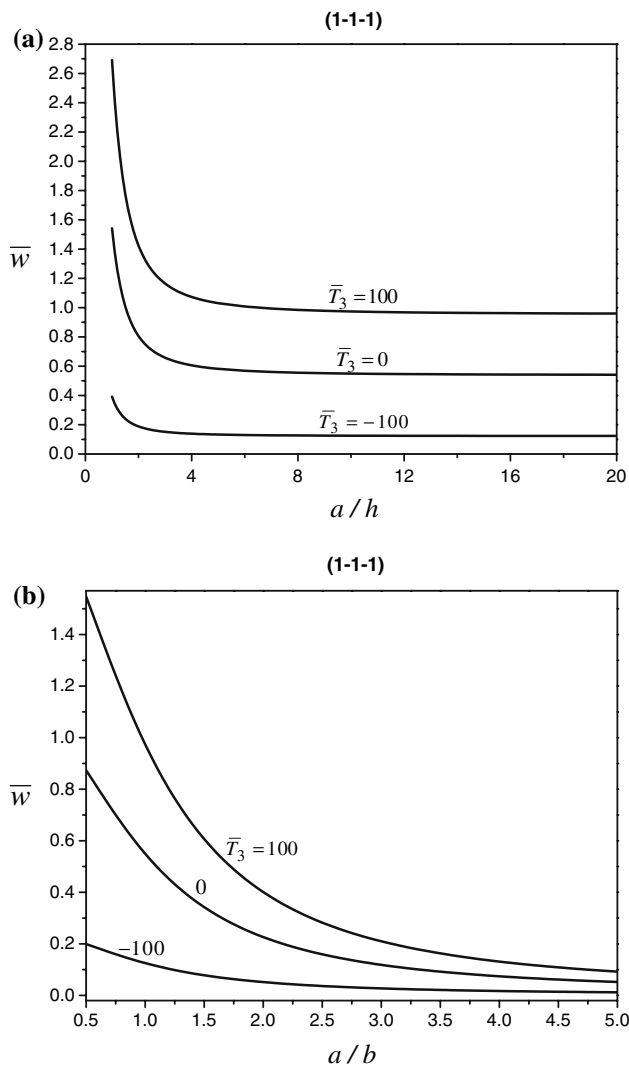


Fig. 7 Effect on thermal load \bar{T}_3 on the dimensionless center deflection \bar{w} of the (1-1-1) FGM sandwich plate ($k = 0.5$): (a) versus a/h , (b) versus a/b

deformation is included in the present theory. The governing equations are converted into a set of coupled ordinary differential equations with variable coefficients. Analytical solutions for FGM sandwich plates are developed using the Navier procedure. The results of the shear deformation theories are compared together. The present SSDPT (with and without the effect of transverse normal strain) offers accurate and reliable solutions for the analysis of homogeneous and FGM sandwich plates comparing with other shear deformation theories. It is seen that the deflection of the plates that correspond to properties intermediate to that of the metal and ceramic necessarily lie in between that of ceramic and metal. The axial stress is found to take the maximum compressive {minimum tensile} at the top {bottom} surface of the core layer.

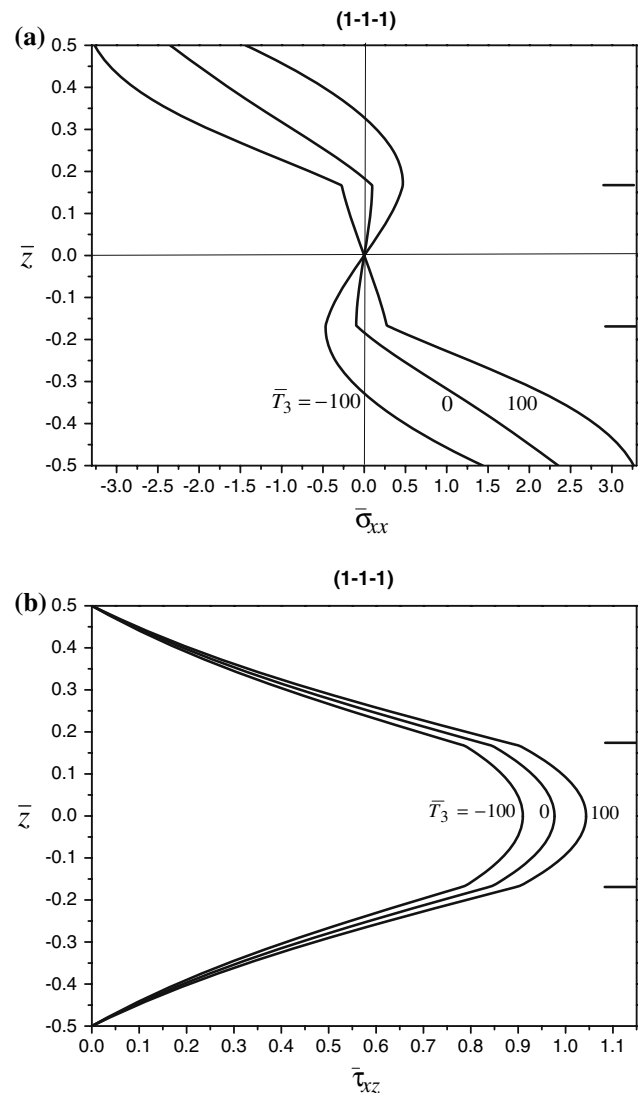


Fig. 8 Effect of the thermal load \bar{T}_3 on (a) axial stress $\bar{\sigma}_{xx}$ and (b) transverse shear stress $\bar{\tau}_{xz}$ of the (1-1-1) FGM sandwich plate ($k = 1.5$)

However, the transverse shear stress is found to take the maximum value at a point on the mid-plane of the FGM plate. Finally, the inclusion of the transverse normal strain will increase the shear stress and will decrease both of deflection and axial stress.

References

1. Timoshenko SP, Woinowsky-Krieger S (1959) Theory of plates and shells. McGraw-Hill, New York
2. Nowacki W (1986) Thermoelasticity. Pergamon, London
3. Boley BA, Weiner JH (1997) Theory of thermal stresses. Dover, New York
4. Wu CH, Tauchert TR (1980) J Therm Stresses 3:247
5. Wu CH, Tauchert TR (1980) J Therm Stresses 3:365
6. Tauchert TR (1980) J Therm Stresses 3:117

7. Pell WH (1946) *Q Appl Math* 4:27
8. Stavsky Y (1963) *J Eng Mech Div Proc ASCE* 89:89
9. Reddy JN, Hsu YS (1980) *J Therm Stresses* 3:475
10. Khdeir AA, Reddy JN (1991) *J Therm Stresses* 14:419
11. Chandrashekhara K (1992) *Finite Elem Anal Des* 12:51
12. Chandrashekhara K, Tenneti R (1994) *Compos Sci Technol* 51:85
13. He J (1995) *Compos Struct* 30:51
14. Wetherhold R, Wang J (1996) *Compos Part B Eng* 27:51
15. Wetherhold R, Seelman S, Wang J (1996) *Compos Sci Technol* 56:1099
16. Fares ME, Zenkour AM (1999) *J Therm Stresses* 22:347
17. Zenkour AM, Fares ME (2000) *J Therm Stresses* 23:505
18. Zenkour AM (2007) *Arch Appl Mech* 77:197
19. Reddy JN (2000) *Int J Numer Meth Eng* 47:663
20. Zenkour AM (2004) *Acta Mech* 171:171
21. Zenkour AM (2004) *Compos Struct* 65:367
22. Zenkour AM (2004) *J Eng Math* 50:75
23. Zenkour AM (2005) *Int J Solids Struct* 42:5224
24. Zenkour AM (2005) *Int J Solids Struct* 42:5243
25. Zenkour AM (2006) *Appl Math Model* 30:67